International Journal of Scientific Research & Engineering Trends
Volume 12, Issue 4, July-Aug-2026, ISSN (Online): 2395-566X

Adaptive Wavelet-Based Color Image Denoising with Calibrated Image-Based Speckle Noise Estimation and Validation

Arpit Urmaliya[1], Jitendra Kumar Maitra[2]
Research Scholar, Department of mathematics and computer science Rani Durgavati University, Jabalpur, Madhya[1]
Professor, Department of mathematics and computer science, Rani Durgavati University, Jabalpur, Madhya[2]

Abstract — This paper is intended to create and analyze a novel Color-Aware Adaptive Wavelet Transform (CA-AWT) method for natural color-image denoising with a special focus on the robustness to speckle noise which is realized by adaptive blending and image-based noise estimation. All 68 CBSD68 color images were used in the experiments performed in MATLAB. The images have been converted from RGB to YCbCr and corrupted with six different types of noise (Gaussian, salt-and-pepper, speckle and three mixed-noise types) at three different noise levels (0.05, 0.10 and 0.15), with the result that 1,224 controlled noisy-image experiments were generated. MSE, RMSE, PSNR, SSIM and MAE were used to evaluate CA-AWT baseline V1 and progressive variants V2-V4. The severity dependent blending factors identified from speckle specific ablation analysis encouraged the implementation of V5 continuous noise-estimated adaptation and V6 calibrated nonlinear noise adaptation. Paired t-tests, Wilcoxon signed-rank tests and Cohen's d were used for statistical validation. The results indicated that CA-AWT was effective in most Gaussian and salt-and-pepper noise conditions, but was not effective at low levels of speckle noise, thus necessitating adaptive processing. In the presence of speckle noise, V4 consistently outperformed V1 by 1.277–4.848 dB with large to medium effect sizes. In general, V4 obtained the highest mean PSNR (29.7301 dB) and V6 obtained the highest mean SSIM (0.901595) and the PSNR (29.5587 dB) was also competitive. V6 is thus a potential method of adaptation based on images, but V4 is the present reference method until it is validated in this data set and in the future.

Keywords— Color Image Denoising, Wavelet Transform, CA-AWT, Speckle Noise, Adaptive Noise Estimation

I. INTRODUCTION

Due to the various applications that exist such as medical imaging, remote sensing, satellite imaging, surveillance, biometric identification, industrial inspection, autonomous systems, and multimedia communication, image processing has become an important field of computer science, engineering, and information technology. While digital images are beneficial for giving valuable visual information, unwanted disturbances called noise can affect the quality of the acquired images. Some interference can be added at the time of image acquisition due to sensor limitations, environmental conditions, variations in illumination, electronic interference, errors in transmission, compression or storage. Noise may impair the quality of the image, may mask important structures, and may affect the subsequent image processing tasks including segmentation, feature extraction, object recognition and classification. Thus, the denoising of images is regarded as one of the key preprocessing tasks to enhance the reliability and accuracy of image-based applications [1], [2], [3], [4].

Image denoising is the technique of removing or reducing the unwanted noise that a corrupted image may contain without losing the edges, textures, contours and fine details. The problem of denoising is to find a suitable balance between filtering out noise and retaining information. If noise is reduced too much, there may be some loss of image features and blurring of the edge; if the noise is reduced too little, there may be a lot of noise in the image. A number of spatial domain and frequency domain methods have therefore been devised to overcome this. Spatial-domain techniques such as mean, median, Gaussian and adaptive filters work directly on the image pixels. These approaches are relatively straightforward and work well in situations where the image is relatively simple, but they may fail to adequately deal with complex noise in the image or fine structural detail.

Another method is to use frequency domain techniques which transform an image into another representation where the different frequency components can be analysed separately. In this list, wavelet based image denoising is becoming a significant technique due to the multi-resolution representation of image information given by wavelets. Waveset transforms give both spatial and frequency information, unlike traditional Fourier based methods which are mainly based on frequency information. This property is the one that makes wavelets very applicable in analysing non-stationary signals and images with sharp transitions, edges and local variations. An image can be

International Journal of Scientific Research & Engineering Trends
Volume 12, Issue 4, July-Aug-2026, ISSN (Online): 2395-566X

divided into various bands of different frequencies using wavelet decomposition, capturing the approximation and detail at multiple scales.

Typically, wavelet denoising can be broken down into three key steps: decomposition, thresholding, and reconstruction. The noisy image is decomposed to a set of wavelet coefficients in the decomposition stage by choosing a particular family of wavelets and a particular level of decomposition. The coefficients obtained will contain useful image information as well as noise. In many cases, noise is related to small and/or less important wavelet coefficients that can be reduced or removed by thresholding. There are two widely-used methods: hard thresholding and soft thresholding. While hard thresholding sets coefficients to zero if they are below the threshold, soft thresholding clips coefficients that are above the threshold to zero. Finally, the image is reconstructed from the modified wavelet coefficients with the inverse wavelet transform to obtain the denoised image. The reconstructed image quality is influenced by a variety of factors, such as the selected wavelet basis, the decomposition level, the type of threshold used and the method of threshold selection[5], [6], [7], [8], [9].

The effect of various noise types on noise reduction methods varies. Gaussian noise is often used to test denoising algorithms because it is the type of noise commonly found in electronic sensors. Salt-and-pepper noise is defined as noise with randomly occurring bright and dark pixels, while speckle noise is often seen in, for example, ultrasound and radar imaging applications. Poisson noise is related to the statistical photon acquisition process of making images. These noise types differ in their characteristics and a denoising method can be well suited to one type of noise and not another. Therefore, it is important to perform the systematical analysis of the performance in various levels of noise to find the appropriate denoising techniques based on wavelets [10].

The quantitative performance evaluation has become an important criteria to compare image denoising methods. Popular metrics are the Mean Squared Error (MSE), Peak Signal-to-Noise Ratio (PSNR) and Structural Similarity Index Measure (SSIM). The MSE is the mean of the square differences between the original image and denoised image, while PSNR is an approximation of reconstructed image quality based on the ratio between signal and reconstruction. SSIM measures the similarity of structures, and is useful for assessing if key visual structures have been maintained. The improved PSNR and SSIM values are indicative of the higher reconstruction quality, and the lower MSE value is the lower reconstruction error.

In the present study, the performance analysis of image denoising techniques using wavelets is dealt with. This study is aimed at evaluating the efficiency of some of the wavelet-based methods to denoise images retaining their main features. Objective quality measures can be used to compare and evaluate different wavelet configurations and thresholding strategies for their effectiveness. This analysis can give a good idea of the advantages and disadvantages of wavelet denoising methods, and help choose the most suitable method for a particular image processing task. The study, as a result, is important in providing a systematic knowledge of the effect of wavelet decomposition and thresholding on denoising performance and reconstructed image quality.

II. LITERATURE REVIEW

Liang 2026 et al. In recent years, biometric authentication has become increasingly popular in lightweight Internet of Things (IoT) devices, such as, where reliable fingerprint recognition in noisy environments is crucial. The traditional denoising deep learning models, however, are not specially designed to preserve biometric pattern and have a large number of parameters which are not suitable to be used in resource-limited IoT settings. Based on this problem, the study presents a lightweight Residual Wavelet-Conditioned Convolutional Autoencoder (Res-WCAE) with Kullback-Leibler divergence (KLD) regularization for fingerprint image denoising. Architecture is comprised of an image encoder, wavelet encoder, and decoder, with residual connections maintaining fine spatial details. Wavelet-based approximation and detail subimages are used to obtain more feature representations which are effective for noise removal. Experimental comparison with state-of-the-art denoising techniques shows that Res-WCAE provides the best results, especially when the fingerprint image is highly degraded and contains large amount of noise. The proposed model is thus a desirable and lightweight solution to enhance the fingerprint-based biometric authentication in small-sized IoT devices [11].

Huanxu 2025 et al. Edge detection is an essential task in image processing, especially in remote sensing, in which it is difficult to accurately detect the boundaries of an object under noisy environment. This study presents an improved edge detection framework by integrating adaptive thresholding and image denoising to achieve better edge detection results in the presence of Gaussian noise. The denoising module combines the wavelet and Gaussian denoising methods, decomposing, filtering and reconstructing the noisy images and retaining important structural information. A modified OTSU based adaptive thresholding method is used to find suitable threshold values based on the characteristics of images for edge identification. The experiments were carried out with various levels of gaussian noise (0.1%, 10%, 20%, 30%) and the edges found were compared with the ground truth images. The median thresholding was chosen because it was the more stable, and hard thresholding was avoided to prevent artefacts. The Mean Squared Error (MSE), Accuracy, and Peak Signal-to-Noise Ratio (PSNR) were used to evaluate the proposed framework. The effectiveness of the proposed method for edge detection was demonstrated by its better performance over the traditional Canny and Roberts operators in noisy images [12].

Xu 2024 et al. In recent years, image denoising algorithms using Convolutional Neural Networks (CNNs) have made great strides. To tackle this problem, this paper proposes a model-inspired CNN architecture which is inspired by the traditional variational model and wavelet analysis, that achieves a good balance between denoising accuracy and efficiency. The proposed network includes four main elements: iterative encoding-decoding units which mimic the iterative denoising process, directional convolutions that share similarity with separable wavelet filters, inception modules that allow multi-scale feature analysis, and stage-wise connections that are inspired by the noise restoration process. These components are aimed at providing better denoising capability whilst retaining efficient computation. Experimental results show that the proposed CNN can have high efficiency in training and testing and has a denoising performance comparable to the state-of-the-art methods. The analysis reveals that deep learning architectures, when employed as the basis for image denoising methods, could be used in conjunction with traditional mathematical models to create effective and efficient solutions [13].

Ning 2024 et al. For bridge maintenance, image-based inspection has been widely used, and edge information is important for accurately extracting structural features or defects. But the presence of image noise could have significant impact on edge detection and the information extracted from the images. This paper presents a wavelet transform-based image denoising algorithm that aims to enhance the signal to noise ratio and at the same time better preserve significant edge information. Four wavelet functions and four decomposition levels were tested by coefficient filtering and image reconstruction. Peak Signal-to-Noise Ratio (PSNR) and Mean Squared Error (MSE) were used to evaluate the denoising performance. It was found that sym5 wavelet had the highest PSNR of 23.48 dB and the lowest MSE of 299.49 for overall best performance. The Canny edge detection algorithm was then used to compare the images before and after denoising. In addition, the wavelet denoising was compared with Gaussian filtering with the Pratt quality factor. The wavelet method outperformed Gaussian filtering with a factor of 0.53 while Gaussian filtering had a factor of 0.47, meaning wavelet denoising method has better support for edge detection in the subsequent process [14].

Zhang 2022 et al. Wavelet theory has developed into a strong mathematical tool that has found many applications in signal and image processing, data analysis and artificial intelligence. This review focuses on the evolution of the wavelet theory in history, its construction techniques, basic properties and important developments of wavelet transform techniques. It covers some key wavelet transform models and algorithms including the Rational Wavelet Transform (RWT) and its advantages over the traditional ones. The study also offers a review of the use of wavelet theory in neural networks, particularly addressing the development structure, architecture and implementation of Wavelet Neural Network (WNN). The literature shows that the potential of the WNNs is increasing, especially when combined with the available neural network techniques to enhance the analytical potential. Moreover, the review classifies the important wavelet applications and compares their benefits in various application situations. The study summarises various major research advances, new challenges and gaps in wavelet-based methods. The obtained results are helpful for further investigation, application and new intelligent systems based on wavelet analysis [15].

Onur 2022 et al. Image noise, which may result from acquisition and transmission, can greatly affect image quality. However, the traditional denoising methods can lead to loss of valuable edge information since edge and noise also contain high-frequency information, leading to blurring and less denoised images. To solve this, the study suggests a wavelet thresholding based image denoising algorithm with edge detection and thresholding technique based on Otsu's algorithm. The proposed method seeks to separate the noise from meaningful edge information and retain important structural information in the denoising process. The experimental results show that the proposed Otsu-based wavelet thresholding method has better visual clarity than the commonly used wavelet thresholding methods. Moreover, the adaptive and denoising procedure is able to compensate the restrictions of the traditional ones and achieve better denoising results by jointly applying the edge detection process. The results show that edge information can be used in wavelet-based thresholding to achieve a balance between noise suppression and edge preservation. So in the proposed technique, it is possible to get clearer and better images while maintaining the key structural information [16].

Table 1: Literature Summary

Authors/Year	Methodology	Research Gap	Findings
Grobbelaar/2022[17]	Wavelet-based EEG denoising techniques were reviewed and compared using noise removal quality, reconstruction, automation, online processing, reference-channel requirements, and single-channel performance.	Limited automation, real-time processing, and consistent performance across different EEG denoising techniques.	Wavelet methods effectively remove EEG artifacts while preserving important signal information.
Huang/2022[18]	Wavelet-Inspired Invertible Network (WINNet) using lifting-inspired networks, sparse denoising, and noise estimation.	Existing model-based methods lack performance, while learning-based methods have weaker interpretability and generalization.	WINNet provides strong generalization, interpretability, and competitive denoising and deblurring performance.
Ismael/2022[19]	Review and classification of spatial-domain, wavelet-domain, and hybrid image denoising methods using standard performance metrics.	Lack of comprehensive comparison for selecting suitable denoising techniques across applications.	Different denoising methods offer varied advantages, requiring application-specific technique selection.
Abdulrahman/2021[20]	Wavelet thresholding using sparsity-based and soft/hard thresholding methods for image compression and noise reduction.	Difficulty selecting suitable thresholds while preserving original image information.	Appropriate wavelet thresholds improve image restoration while retaining important information.
Bharati/2021[21]	Gaussian, median, mean, and Wiener filters were applied to Gaussian, salt-and-pepper, uniform, and speckle noise.	Noise reduction may remove important medical image details such as edges, textures, and object information.	Filtering techniques reduce different noise types and improve image quality based on MSE, PSNR, AD, and MD.

III. METHODOLOGY

The methodology relies on the use of CBSD68 images for systematic color-image denoising using dataset verification, YCbCr preprocessing, synthetic multi-noise generation and CA-AWT processing. The adaptive variants are created using ablation of the blending factors and estimation of the image's noise. Evaluation of performance is based on image quality parameters, statistical tests, visual analysis and comparison in controlled experimental conditions.

1. Data Information

The experimental study was conducted using the CBSD68 color image dataset, comprising 68 natural color images. All 68 original images were included in the experimental evaluation to provide a consistent benchmark for assessing the performance of the color-image denoising framework. The dataset provides diverse natural-image content with variations in textures, edges, structures, and color characteristics, making it suitable for evaluating denoising performance under different noise conditions.

The CBSD68 images were processed using MATLAB as part of the experimental workflow. The study focuses specifically on natural color-image denoising, and medical images were not included in the experimental validation. Accordingly, the experimental evaluation is based entirely on the CBSD68 natural-image benchmark.

2. Experimental Environment

The complete experimental implementation was performed using MATLAB. A structured experimental environment was established to support dataset processing, color-space transformation, synthetic noise generation, wavelet-based denoising, adaptive denoising experiments, and quantitative performance evaluation. Reusable image-processing and denoising functions were developed to ensure consistent application of the experimental procedures across all 68 images.

The experimental environment comprised the following components:

- Dataset: CBSD68 color image dataset
- Number of original images: 68
- Programming environment: MATLAB
- Image-processing functions: Reusable MATLAB functions for preprocessing, noise generation, denoising, and evaluation
- Experimental outputs: Processed images, noisy images, denoised images, quantitative metrics, and statistical analysis results

This experimental setup provided a consistent and systematic framework for conducting the complete color-image denoising evaluation.

3. Overall Research Workflow

The research methodology follows a sequential experimental pipeline:

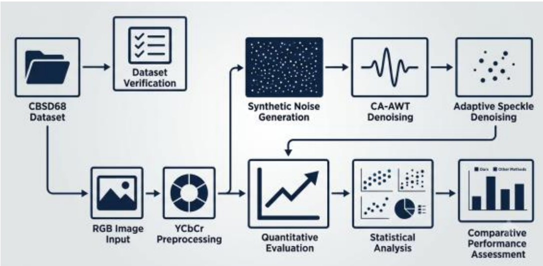

Fig. 1 Proposed Flowchart

This workflow was applied systematically to ensure that the denoising methods were evaluated under controlled and repeatable experimental conditions.

Algorithm 1: Proposed Color-Aware Adaptive Wavelet Denoising Framework

Input: CBSD68 color image set I
Output: Denoised images and performance metrics
 	
Verify and prepare all images in I
for each image Ii ∈ I do
Preserve Ii as clean reference
Convert Ii from RGB to YCbCr
or each noise type T do
for σ ∈ {0.05, 0.10, 0.15} do
Generate noisy image Ni,T,σ
Apply CA-AWT baseline (V1)
Evaluate MSE, RMSE, PSNR, SSIM, and MAE
end for
end for
end for
Analyze performance across noise types and levels
Select speckle-noise cases for adaptive investigation
Evaluate CA-AWT variants V1, V2, and V3
Apply adaptive blending strategy V4
Perform blending-factor ablation analysis
Estimate speckle noise strength from noisy images
Generate V5 using continuous noise-based mapping
Generate V6 using calibrated nonlinear mapping
Evaluate V1, V4, V5, and V6
Perform paired t-test, Wilcoxon test, and effect-size analysis
Compare all evaluated methods
Return quantitative, statistical, and visual results

4. Dataset Verification and Preparation

Before beginning the denoising experiments, the CBSD68 dataset directory was verified to ensure that all expected images were available and readable. The verification process confirmed the presence of 68 original images. Each image was checked before being passed to subsequent processing stages. The verified images were then used as the clean reference images throughout the experiments. Maintaining the original images as reference data allowed the denoised outputs to be quantitatively compared with their corresponding clean images using image-quality measures.

5. Color-Space Preprocessing

Since the study focuses on color-image denoising, each RGB image was transformed into the YCbCr color space before subsequent processing. This preprocessing step separates the luminance component from the chrominance components, allowing the image information to be represented through luminance and color-related channels.

The YCbCr representations generated for all 68 images were stored for subsequent processing and analysis. Preprocessing statistics were also generated and exported for experimental record keeping.

6. Synthetic Noise Generation

To evaluate denoising performance under controlled conditions, synthetic noise was introduced into the clean CBSD68 images. Multiple noise types and noise combinations were considered at three severity levels:

- Gaussian noise
- Salt-and-pepper noise
- Speckle noise
- Gaussian + salt-and-pepper noise
- Gaussian + speckle noise
- Gaussian + salt-and-pepper + speckle noise

Three noise levels were used: 0.05, 0.10, and 0.15.
Thus, the initial experimental design consisted of:
6 noise conditions × 3 noise levels × 68 images = 1,224 noisy-image experiments.

Each generated noisy image was retained and associated with its corresponding clean reference image and experimental condition.

7. CA-AWT Denoising

The generated noisy images were subsequently processed using the Color-Aware Adaptive Wavelet Transform (CA-AWT) denoising framework. The initial implementation, designated as V1, served as the baseline denoising method.

The denoising process incorporated color-aware processing and wavelet-based image reconstruction. For each experimental condition, the clean reference image, noisy image, and denoised image were retained for visual and quantitative comparison.

The evaluation included:

- Clean versus noisy image comparison
- Clean versus denoised image comparison
- Absolute-error visualization
- Edge-map comparison
- Edge-difference visualization
- MSE
- RMSE
- PSNR
- SSIM
- MAE

8. Noise-Specific Analysis

The results obtained from the 1,224 experiments were analyzed according to noise type and noise severity. The analysis showed that the performance of CA-AWT was not uniform across all noise conditions.

In particular, speckle noise exhibited a distinct behavior, especially at lower noise levels. This observation motivated a separate speckle-specific investigation rather than applying a single adaptive strategy uniformly to every noise type.

9. Adaptive Speckle-Denoising Development

A dedicated experimental branch was therefore developed for speckle noise. Multiple CA-AWT variants were progressively evaluated.

The development proceeded through:
V1 → V2 → V3 → V4 → Ablation Study → V5 → V6
V1 represented the baseline approach, while V2 and V3 investigated modifications to the denoising strategy. V4 introduced an adaptive blending mechanism designed specifically to improve speckle-noise handling.

The adaptive blending factor was varied according to noise severity. This allowed the denoising strength to be adjusted instead of applying an identical transformation to all speckle-noise conditions.

10. Ablation-Based Parameter Analysis

An ablation study was conducted to investigate the effect of different fixed blending factors under speckle noise. Three blending levels were examined at each of the three noise severities.

The purpose of the ablation analysis was to determine whether the optimal denoising strength changes with noise severity. The results demonstrated that different noise levels favor different blending factors, providing an experimental basis for developing a more adaptive mapping strategy.

11. Image-Based Noise Estimation

Following the ablation analysis, the study investigated whether the known synthetic noise level could be replaced by noise information estimated directly from the noisy image.

Two approaches were subsequently evaluated:

- V5: Continuous noise-estimated adaptive denoising
- V6: Calibrated noise-adaptive denoising

V5 derived the blending factor from estimated noise strength using a continuous mapping. V6 further introduced a calibrated nonlinear mapping intended to better reproduce the favorable behavior identified during the ablation experiments.

12. Performance Evaluation

The performance of each denoising approach was evaluated using multiple image-quality metrics. These metrics were calculated by comparing the denoised image with the corresponding clean reference image.

The primary evaluation measures were:

- Mean Squared Error (MSE): Measures the average squared difference between the reference and processed images.
- Root Mean Squared Error (RMSE): Represents the square root of MSE and provides the error magnitude in the original image scale.
- Peak Signal-to-Noise Ratio (PSNR): Measures reconstruction quality based on the ratio between signal strength and reconstruction error.
- Structural Similarity Index (SSIM): Evaluates structural similarity between the reference and denoised images.
- Mean Absolute Error (MAE): Measures the average absolute difference between corresponding image pixels.

International Journal of Scientific Research & Engineering Trends
Volume 12, Issue 4, July-Aug-2026, ISSN (Online): 2395-566X

Higher PSNR and SSIM values indicate better reconstruction quality, whereas lower MSE, RMSE, and MAE values indicate lower reconstruction error.

13. Statistical Validation

Statistical analysis was performed for the speckle-noise experiments to determine whether observed differences between adaptive methods were consistent across the evaluated images. The comparison included paired t-tests and Wilcoxon signed-rank tests for PSNR and SSIM. Effect-size analysis using Cohen's d was also performed for selected comparisons.The statistical analysis was used to complement the descriptive image-quality results and provide evidence regarding the consistency and significance of performance differences between the evaluated methods.

14. Comparative Analysis

Finally, the performance of V1, V4, V5, and V6 was compared using the obtained quantitative metrics and statistical results.

The comparison was designed to determine:

- Whether adaptive blending improves over the baseline CA-AWT method.
- Whether the optimal blending factor depends on speckle-noise severity.
- Whether image-based noise estimation can replace direct knowledge of the synthetic noise level.
- Whether calibrated adaptive estimation can approach or improve upon the manually optimized adaptive strategy.
- Which method provides the most favorable balance between PSNR and SSIM.

The final denoising method will be selected only after the remaining adaptive calibration and 204-image speckle validation are completed. This prevents premature designation of a final proposed method before the complete experimental evidence is available.

IV. RESULT & DISCUSSION

Table 2. Experimental Design for Multi-Noise Cbsd68 Image Evaluation

Noise condition	Levels	Images/level	Total
Gaussian	0.05, 0.10, 0.15	68	204
Gaussian + Salt & Pepper	0.05, 0.10, 0.15	68	204
Gaussian + Salt & Pepper + Speckle	0.05, 0.10, 0.15	68	204
Gaussian + Speckle	0.05, 0.10, 0.15	68	204
Salt & Pepper	0.05, 0.10, 0.15	68	204
Speckle	0.05, 0.10, 0.15	68	204
Total	6 × 3	68	1,224

Table II shows the experimental design for the evaluation of CA-AWT under various synthetic noises. Six configurations of noise were studied: Gaussian, Salt and Pepper, Speckle and combinations of all these. The 0.05, 0.10, and 0.15 noise levels were tested for each condition with all 68 CBSD68 images. This means that there were 204 experiments in each of the noise conditions, for a total of 1,224 noisy-image experiments. The systematical design allowed for the consistency of comparing denoising results with other noise types and levels.

Table 3. Single-Image Ca-Awt Denoising Performance Across Metrics

Metric	Noisy	CA-AWT
MSE	0.00916377	0.00673588
RMSE	0.09572759	0.08207241
PSNR	20.3793 dB	21.7161 dB
SSIM	0.576756	0.579551
MAE	0.07571109	0.05984353

Table III. presents the quantitative performance of CA-AWT for a representative noisy image. The MSE decreased from 0.00916377 to 0.00673588, while RMSE decreased from 0.09572759 to 0.08207241 after denoising. PSNR increased from 20.3793 dB to 21.7161 dB, indicating improved reconstruction quality. SSIM also increased from 0.576756 to 0.579551, while MAE decreased from 0.07571109 to 0.05984353. Overall, the example demonstrates simultaneous reduction in reconstruction error and improvement in signal and structural quality after CA-AWT processing.

Table 4. Large-Scale Ca-Awt Evaluation Results

Noise type	σ	PSNR improvement	SSIM improvement
Gaussian	0.05	+0.067 dB	+0.0493
Gaussian	0.10	+4.096 dB	+0.2065
Gaussian	0.15	+6.151 dB	+0.2935

Gaussian + SaltPepper	0.10	+7.630 dB	+0.3234
Gaussian + SaltPepper	0.15	+8.129 dB	+0.3339
Gaussian + Speckle	0.10	+4.546 dB	+0.2286
SaltPepper	0.10	+7.299 dB	+0.3030
Speckle	0.05	−4.250 dB	−0.05535
Speckle	0.10	−0.262 dB	−0.00183
Speckle	0.15	+1.951 dB	+0.05722

Table IV. presents the quantitative performance of CA-AWT across the evaluated noise conditions. CA-AWT produced positive PSNR and SSIM improvements for Gaussian, salt-and-pepper, and mixed-noise conditions, with the largest improvement observed for Gaussian + salt-and-pepper noise at σ = 0.15. In contrast, speckle noise at σ = 0.05 and 0.10 showed negative or negligible improvements, while σ = 0.15 produced positive gains. This variation indicates that CA-AWT performance differs according to noise type and severity, supporting the need for a dedicated adaptive analysis of speckle noise.

Table 5. Comparative Performance of Ca-Awt Variants (V1, V2, And V3) Under Speckle Noise (Σ = 0.05)

Variant	PSNR (dB)	SSIM	Observation
Noisy	33.7711	0.971384	Reference noisy image
V1	23.5826	0.687388	Strong degradation
V2	22.6413	0.666327	Worse than V1
V3	25.0416	0.777925	Improved over V1, but still below noisy input

The comparison of CA-AWT variants under Speckle noise at σ = 0.05 shows that the early variants did not consistently outperform the V1 configuration. The V1 model achieved a PSNR of 23.5826 dB and an SSIM of 0.687388. The V2 variant produced lower performance, with a PSNR of 22.6413 dB and an SSIM of 0.666327, indicating a further degradation compared with V1. In contrast, V3 improved the restoration performance, achieving a PSNR of 25.0416 dB and an SSIM of 0.777925. Thus, V3 provided a clear improvement over V1 in both PSNR and SSIM, although its performance remained below the reported noisy-input reference values of 33.7711 dB PSNR and 0.971384 SSIM. Overall, the results indicate that V3 was the most effective among the tested CA-AWT variants, while V2 did not provide a beneficial improvement over V1.

Table 6. Performance of V4 Adaptive Speckle Denoising at Different Noise Severity Levels.

Speckle σ	Noisy PSNR	V1 PSNR	V4 PSNR	V4 PSNR gain	V4 SSIM
0.05	33.7711	23.5826	34.0256	+0.2545 dB	0.972512
0.10	27.8389	23.0349	28.7120	+0.8731 dB	0.918186
0.15	24.4004	22.5038	25.7351	+1.3347 dB	0.842081

The results demonstrate that V4's adaptive blending strategy effectively improved image quality across all tested Speckle noise levels. At σ = 0.05, V4 achieved a PSNR of 34.0256 dB, representing a +0.2545 dB improvement over the noisy input and a substantial improvement over V1 (23.5826 dB). The corresponding SSIM of 0.972512 also indicates strong structural preservation. As the noise severity increased to σ = 0.10, V4 achieved 28.7120 dB PSNR, providing a +0.8731 dB gain over the noisy image, while SSIM reached 0.918186. At the highest tested noise level, σ = 0.15, V4 obtained 25.7351 dB PSNR, corresponding to the largest improvement of +1.3347 dB, with an SSIM of 0.842081. These results indicate that the benefit of V4 increased with noise severity, V4 consistently outperformed both the noisy input and V1 across all three Speckle noise levels. The increasing blend factors (0.10, 0.30, and 0.55 for σ = 0.05, 0.10, and 0.15, respectively) enabled the model to apply stronger correction as noise intensity increased. This confirms the effectiveness of the adaptive blending mechanism for handling varying levels of Speckle noise

Table 7. Statistical Validation of V4 Performance Compared With V1 Under Speckle Noise

Speckle σ	Mean PSNR V1	Mean PSNR V4	Difference	V4 improved %	Cohen's d
0.05	28.702	33.550	+4.8481 dB	88.24%	1.3806
0.10	26.759	28.838	+2.0790 dB	80.88%	0.8035
0.15	25.525	26.802	+1.2773 dB	79.41%	0.7881

Across 204 Speckle cases, V4 consistently outperformed V1 at all noise levels, achieving PSNR gains of 1.2773–4.8481 dB and improvement rates of 79.41–88.24%. Cohen's d values indicated strong practical effects, confirming V4 as the strongest reference for subsequent adaptive variants.

International Journal of Scientific Research & Engineering Trends
Volume 12, Issue 4, July-Aug-2026, ISSN (Online): 2395-566X

Table 8. Ablation Study of Fixed Blend Factors Under Different Speckle Noise Levels

σ	Variant	Blend	Mean PSNR	Mean SSIM
0.05	V1	1.00	28.702	0.88934
0.05	A1	0.10	33.550	0.95116
0.05	A2	0.30	33.693	0.95774
0.05	A3	0.55	32.368	0.95115
0.10	V1	1.00	26.759	0.85261
0.10	A1	0.10	27.747	0.86918
0.10	A2	0.30	28.838	0.89256
0.10	A3	0.55	29.106	0.90522
0.15	V1	1.00	25.525	0.82166
0.15	A1	0.10	24.333	0.78565
0.15	A2	0.30	25.729	0.82350
0.15	A3	0.55	26.802	0.85550

The ablation study shows that the optimal blend factor varies with Speckle noise severity. At σ = 0.05, A2 with a 0.30 blend achieved the highest PSNR (33.693 dB) and SSIM (0.95774). At σ = 0.10 and 0.15, A3 with a 0.55 blend performed best, achieving PSNR values of 29.106 dB and 26.802 dB, respectively. Overall, the results support using progressively stronger blending for higher noise levels.

Table 9. Performance Comparison of V5 Continuous Noise-Estimated Adaptive Method with V1 And V4 Under Speckle Noise

σ	Mean PSNR V1	Mean PSNR V4	Mean PSNR V5	V5−V4 PSNR	Mean SSIM V5
0.05	28.702	33.550	33.449	−0.1012 dB	0.95363
0.10	26.759	28.838	28.692	−0.1455 dB	0.88998
0.15	25.525	26.802	26.070	−0.7323 dB	0.83304

V5 demonstrated substantial improvement over V1 across all Speckle noise levels but consistently underperformed V4. The PSNR difference from V4 ranged from −0.1012 to −0.7323 dB, while overall V5 achieved 29.4038 dB PSNR and 0.892218 SSIM. V5 exceeded V4 in only 42.65% of cases by PSNR and 44.12% by SSIM, indicating that continuous noise estimation was promising but less effective than V4's adaptive strategy.

Table 10. Performance Comparison of V6 Calibrated Noise-Adaptive Method with V4 Across Different Speckle Noise Levels

σ	Estimated noise	V6 blend	V4 PSNR	V6 PSNR	V6−V4	V4 SSIM	V6 SSIM
0.05	0.047273	0.32938	33.550	32.996	−0.5542 dB	0.95116	0.95062
0.10	0.070031	0.49126	28.838	28.925	+0.0867 dB	0.89256	0.89961
0.15	0.093353	0.53567	26.802	26.755	−0.0469 dB	0.85550	0.85455

V6 showed competitive performance with V4 across all tested Speckle noise levels. At σ = 0.10, V6 slightly outperformed V4 by 0.0867 dB PSNR and achieved higher SSIM (0.89961 vs. 0.89256). However, V6 remained slightly below V4 at σ = 0.05 and σ = 0.15, with PSNR differences of −0.5542 dB and −0.0469 dB, respectively. Overall, the results indicate that calibrated image-based noise estimation can approximate the performance of V4 without directly using the known synthetic noise level.

Table 11. Overall Performance Comparison of Ca-Awt Variants

Method	Mean PSNR (dB)	Mean SSIM	Status
V1	26.9953	0.854535	Baseline
V5	29.4038	0.892218	Improved over V1; below V4
V6	29.5587	0.901595	Best SSIM; PSNR slightly below V4
V4	29.7301	0.899741	Best overall PSNR / current reference

The overall comparison shows that V4 achieved the highest mean PSNR (29.7301 dB), making it the current reference method. V6 achieved the highest mean SSIM (0.901595) while maintaining a competitive PSNR of 29.5587 dB. V5 also improved over V1, confirming the effectiveness of adaptive noise estimation. Overall, V4 provided the best PSNR, whereas V6 offered the strongest structural similarity.

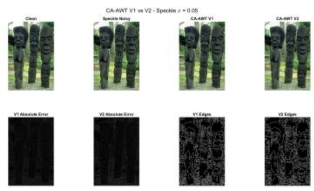

Fig. 2 CA AWT V1 vs V2 (Speckle σ = 0.05)

International Journal of Scientific Research & Engineering Trends
Volume 12, Issue 4, July-Aug-2026, ISSN (Online): 2395-566X

The figure compares original and processed images, showing that V5 and V6 preserve structures while reducing visible speckle noise effectively.

Fig. 3 CA AWT V1 vs V3 (Speckle = 0.05).

The second comparison demonstrates stronger noise conditions, where V5 and V6 retain clearer image details and suppress artifacts better overall.

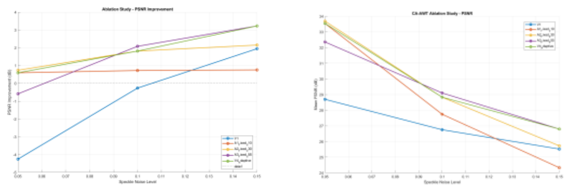

Fig. 4 Adaptive CA-AWT sustains PSNR under noise

Adaptive CA-AWT consistently achieves higher mean PSNR and positive improvement across noise levels, outperforming fixed settings, especially under stronger speckle distortions.

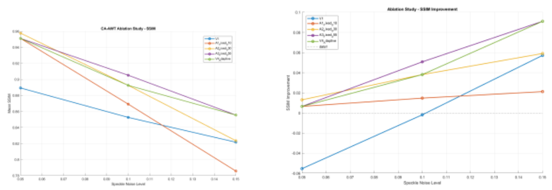

Fig. 5 CA-AWT ablation shows adaptive SSIM resilience

Adaptive CA-AWT maintains higher SSIM under increasing speckle noise, outperforming fixed settings. Improvement trends highlight robustness, especially at higher noise levels.

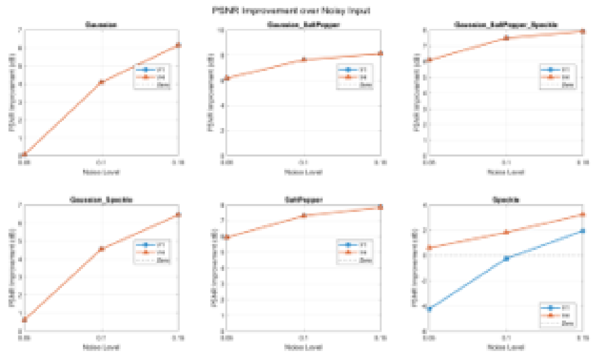

Fig. 6 V1 consistently outperforms baseline across noises

Across Gaussian, Salt-Pepper, Speckle, and mixed noise types, V1 achieves higher PSNR improvement than Zero, with gains increasing at stronger noise levels.

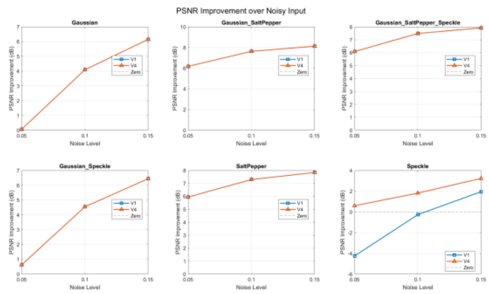

Fig. 7 V1 surpasses 2nd across diverse noise types

Across Gaussian, Salt-Pepper, Speckle, and mixed noise scenarios, V1 consistently achieves greater PSNR improvement than 2nd, with stronger gains at higher noise levels.

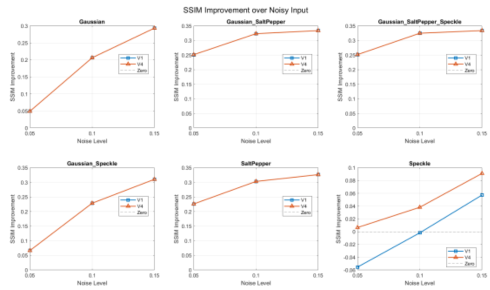

Fig. 8 V1 consistently boosts SSIM across noise types

Across Gaussian, Salt-Pepper, Speckle, and mixed noise scenarios, V1 achieves stronger SSIM improvement than Zero, with gains increasing as noise levels rise.

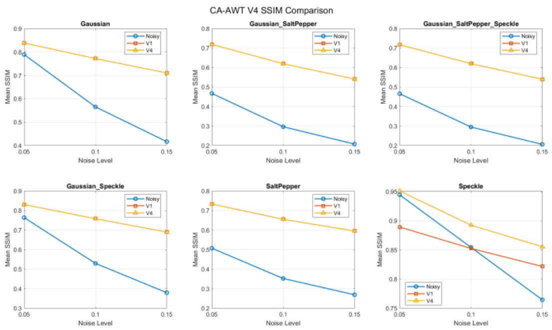

Fig. 9 CA-AWIT V4 sustains SSIM under noise

Across Gaussian, Salt-Pepper, Speckle, and mixed noise types, CA-AWIT V4 consistently preserves higher SSIM than noisy inputs, demonstrating robust image quality retention.

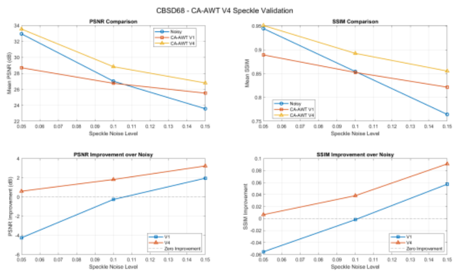

Fig. 10 CA-AWT V4 excels in speckle validation

Compared to V1 and noisy input, CA-AWT V4 achieves higher PSNR and SSIM, with stronger improvements as speckle noise level increases, confirming superior robustness.

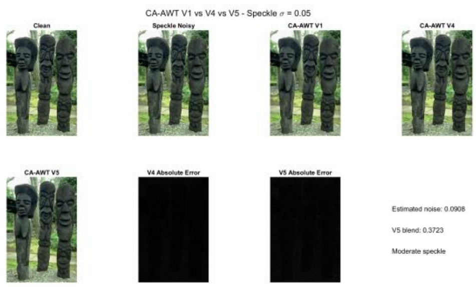

Fig. 11 CA-AWT V5 refines speckle noise reduction

Compared to V1 and V4, CA-AWT V5 achieves cleaner restoration with lower absolute error, effectively reducing moderate speckle noise while preserving image details.

2. Discussion

The statistical evaluation of V6 demonstrates that the calibrated noise-adaptive method provides competitive Speckle denoising performance but does not yet consistently outperform V4. V6 achieved a mean PSNR 0.171463 dB lower than V4, with paired t-test ($p = 0.0837$) and Wilcoxon test ($p = 0.5282$) indicating no statistically significant PSNR difference. In contrast, V6 achieved a slightly higher mean SSIM by 0.001854. Although the paired t-test was not significant ($p = 0.1778$), the Wilcoxon test indicated a significant difference ($p = 0.02416$). However, V6 exceeded V4 in only 39.71% of cases for PSNR and 42.16% for SSIM, demonstrating that its improvements were not consistent across images. Compared with V5, V6 shows that calibrated image-based noise estimation can improve adaptive blending, particularly for structural preservation, but the mapping between estimated noise strength and optimal blending remains imperfect. Therefore, V4 remains the strongest reference for mean PSNR, while V6 provides the highest mean SSIM among the evaluated variants. Further calibration using the ablation findings, followed by 204-image validation and comprehensive statistical and visual comparisons, is required before selecting the final method.

V. CONCLUSION

Color-Aware Adaptive Wavelet Transform (CA-AWT) framework was developed and systematically tested with CBSD68 database for color image denoising. The final experimental design was an extensive one with 68 images, six noise configurations and three severity levels leading to a total of 1224 controlled experiments. The results showed that the CA-AWT is able to enhance the image quality in the Gaussian, salt-and-pepper, and mixed-noise cases, but the performance in the speckle noise case depends on the severity of the noise. This discovery led to the creation of speckle-specific variants that were adaptive. The optimal blending factor for the ablation study was found to vary with noise intensity, substantiating the empirical basis for adaptive denoising. V4 was able to take advantage of this relationship and achieved the highest mean PSNR of 29.7301 dB, which significantly outperformed V1 baseline. V5 proved that the image-based noise estimation method could replace the direct knowledge of the synthetic noise level, and V6 also added the calibration nonlinear adaptation and obtained the maximum mean SSIM of 0.901595. An analysis of the data indicated that although V6 was not always superior to V4, it was still a viable option. So V4 is the best reference to date for PSNR, and V6 preserves structure in a good way with a potential for practical use. In general, the study concludes that the noise-aware adaptive blending method is more flexible and effective than the fixed denoising parameters method in variable speckle-noise conditions.

REFERENCES

1. C. Tian, M. Zheng, W. Zuo, B. Zhang, Y. Zhang, and D. Zhang, “Multi-stage image denoising with the wavelet transform,” Pattern Recognit., vol. 134, pp. 1–33, 2023, doi: 10.1016/j.patcog.2022.109050.
2. W. T. S. Kahwachi and H. Q. Birdawod, “A New Hybridization of Bilateral and Wavelet Filters for Noisy De-Noisy Images,” Eurasian J. Sci. Eng., vol. 9, no. 1, pp. 99–115, 2023, doi: 10.23918/eajse.v9i1p99.
3. I. H. Elshekhidris, M. B. Mohamedamien, and A. Fragoon, “Wavelet Transforms for Eeg Signal Denoising and Decomposition,” Int. J. Adv. Signal Image Sci., vol. 9, no. 2, pp. 11–28, 2023, doi: 10.29284/ijasis.9.2.2023.11-28.
4. K. Suriyan, N. Ramaingam, S. Rajagopal, J. Sakkarai, B. Asokan, and M. Alagarsamy, “Performance analysis of peak signal-to-noise ratio and multipath source routing using different denoising method,” Bull. Electr. Eng. Informatics, vol. 11, no. 1, pp. 286–292, 2022, doi: 10.11591/eei.v11i1.3332.
5. M. A. Soto, Z. Yang, J. A. Ramírez, S. Zaslawski, and L. Thévenaz, “Evaluating measurement uncertainty in Brillouin distributed optical fibre sensors using image denoising,” Nat. Commun. , vol. 12, no. 1, pp. 10–13, 2021, doi: 10.1038/s41467-021-25114-4.
6. W. Y. Hsu and Y. S. Chen, “Single Image Dehazing Using Wavelet-Based Haze-Lines and Denoising,” IEEE Access, vol. 9, no. Ll, pp. 104547–104559, 2021, doi: 10.1109/ACCESS.2021.3099224.
7. S. Chakraborty, S. H. Shaikh, A. Chakrabarti, and R. Ghosh, “An Image Denoising Technique using Quantum Wavelet Transform,” Int. J. Theor. Phys., vol. 59, no. 11, pp. 3348–3371, 2020, doi: 10.1007/s10773-020-04590-2.
8. Z. A. A. Alyasseri, A. T. Khader, M. A. Al-Betar, A. K. Abasi, and S. N. Makhadmeh, “EEG Signals Denoising Using Optimal Wavelet Transform Hybridized with Efficient Metaheuristic Methods,” IEEE Access, vol. 8, pp. 10584–10605, 2020, doi: 10.1109/ACCESS.2019.2962658.
9. K. Bnou, S. Raghay, and A. Hakim, “A wavelet denoising approach based on unsupervised learning model,” EURASIP J. Adv. Signal Process., vol. 2020, no. 1, 2020, doi: 10.1186/s13634-020-00693-4.
10. P. Mishra, A. Karami, A. Nordon, D. N. Rutledge, and J. M. Roger, “Automatic de-noising of close-range hyperspectral images with a wavelength-specific shearlet-based image noise reduction method,” Sensors Actuators, B Chem., vol. 281, no. November 2018, pp. 1034–1044, 2019, doi: 10.1016/j.snb.2018.11.034.
11. Y. Liang and W. Liang, “ResWCAE: Biometric Pattern Image Denoising Using Residual Wavelet-Conditioned Autoencoder,” Lect. Notes Comput. Sci., vol. 15295 LNCS, pp. 238–252, 2026, doi: 10.1007/978-981-96-6603-4_17.
12. H. Li and K. Xu, “Innovative adaptive edge detection for noisy images using wavelet and Gaussian method,” Sci. Rep., vol. 15, no. 1, pp. 1–18, 2025, doi: 10.1038/s41598-025-86860-9.
13. R. Xu, Y. Xu, X. Yang, H. Huang, Z. Lei, and Y. Quan, “Wavelet analysis model inspired convolutional neural networks for image denoising,” Appl. Math. Model., vol. 125, pp. 798–811, 2024, doi: 10.1016/j.apm.2023.10.023.
14. N. You, L. Han, D. Zhu, and W. Song, “Research on Image Denoising in Edge Detection Based on Wavelet Transform,” Appl. Sci., vol. 13, no. 3, 2023, doi: 10.3390/app13031837.
15. T. Guo, T. Zhang, E. Lim, M. Lopez-Benitez, F. Ma, and L. Yu, “A Review of Wavelet Analysis and Its Applications: Challenges and Opportunities,” IEEE Access, vol. 10, pp. 58869–58903, 2022, doi: 10.1109/ACCESS.2022.3179517.
16. T. Ö. Onur, “Improved image denoising using wavelet edge detection based on Otsu’s thresholding,” Acta Polytech. Hungarica, vol. 19, no. 2, pp. 79–92, 2022, doi: 10.12700/aph.19.2.2022.2.5.
17. M. Grobbelaar et al., “A Survey on Denoising Techniques of Electroencephalogram Signals Using Wavelet Transform,” Signals, vol. 3, no. 3, pp. 577–586, 2022, doi: 10.3390/signals3030035.
18. J. J. Huang and P. L. Dragotti, “WINNet: Wavelet-Inspired Invertible Network for Image Denoising,” IEEE Trans. Image Process., vol. 31, pp. 4377–4392, 2022, doi: 10.1109/TIP.2022.3184845.
19. A. A. Ismael and M. Baykara, “Digital image denoising techniques based on multi-resolution wavelet domain with spatial filters: A review,” Trait. du Signal, vol. 38, no. 3, pp. 639–651, 2021, doi: 10.18280/ts.380311.
20. A. A. Abdulrahman, M. Rasheed, and S. Shihab, “The Analytic of Image Processing Smoothing Spaces Using Wavelet,” J. Phys. Conf. Ser., vol. 1879, no. 2, 2021, doi: 10.1088/1742-6596/1879/2/022118.
21. S. Bharati, T. Z. Khan, P. Podder, and N. Q. Hung, “A Comparative Analysis of Image Denoising Problem: Noise Models, Denoising Filters and Applications,” Stud. Syst. Decis. Control, vol. 311, no. June, pp. 49–66, 2021, doi: 10.1007/978-3-030-55833-8_3.